Available online at www.sciencedirect.com

ScienceDirect

Procedia IUTAM 00 (2011) 1–16

Procedia IUTAM

2011 Symposium on Human Body Dynamics

Forward Dynamic Human Gait Simulation using a SLIP Target Model

Matthew Millard[a,*], Eric Kubica[b], John McPhee[a]

[a] *Systems Design Engineering, University of Waterloo, 200 University Ave. West, Waterloo ON N2L 3G1, Canada*
[b] *Electrical and Computer Engineering, University of Waterloo, 200 University Ave. West, Waterloo ON N2L 3G1, Canada*

Abstract

Anthropomorphic multibody models typically have a fragile sense of balance and generate ground reaction force profiles that do not look similar to experimentally measured human ground reaction force profiles. In contrast, the point-mass spring-loaded-inverted-pendulum (SLIP) can be made to walk or run in a balanced manner with center-of-mass kinematics and ground reaction force profiles that could be mistaken for the equivalent human data. A stance limb controller is proposed that uses a planar SLIP to compute a reference trajectory for a planar anthropomorphic multibody gait model. The torso of the anthropomorphic model is made to track the computed trajectory of the SLIP using a feedback control system. The aim of this partitioned approach to gait simulation is to endow the anthropomorphic model with the human-like gait of the simpler SLIP model.

Keywords: Human gait simulation; Multibody gait model; SLIP; Torso tracking

1. Introduction

A predictive, forward-dynamic model and computer simulation of human gait has many important medical and research applications. Most human simulation work has focused on inverse dynamics studies to quantify joint reaction forces and muscle loads [1, 2]. Inverse dynamics is not predictive — it works backwards from experimentally measured motions in an effort to find the forces that caused the motion. Although inverse dynamics is very useful for understanding how a human may have moved during an experiment, this approach inherently masks the principal motivations of balance and locomotion that ultimately led the subject to move in a particular manner. In contrast, forward dynamics determines how a mechanism will move without the need for experimentation, but requires that a suitable control system be formulated to make the model walk (in the case of this paper) in a human-like manner. This paper is focused on testing a candidate control system to allow a multibody gait model to walk in a human like manner at a constant velocity.

*Corresponding author. Tel: +001-519-888-4567 x33825; fax: +001-519-746-4791
Email address: mjhmilla@uwaterloo.ca (Matthew Millard)

The majority of gait controllers developed by the robotics and kinesiology communities are focused on enforcing periodic leg movements typical of walking. The focus on maintaining the periodicity of walking has led to the development of a rigorous theoretical framework for analyzing periodic systems with applied impulses (the impulses occur when the foot models contact the ground), be they robot [3, 4] or human [5]. Many heuristic controllers have also been developed on the assumption that the key feature of walking is the periodicity of the legs [6, 7, 8, 9]. Although the resulting model kinematics of these simulations are in some cases very similar to human joint kinematics, the ground reaction force profiles are vastly different. These differences arise — particularly in [5, 7, 8, 9] due to the use of high-gain feedback control — because the control system is preventing the kinematics of the legs from flexing from the predefined joint trajectories under load, resulting in impulsive ground reaction forces during contact onset that are not characteristic of human ground reaction force profiles [1].

In contrast, the trajectory of the torso can be selected as a control objective allowing the kinematics of the legs to evolve freely during the stance phase, potentially eliminating spurious ground reaction forces. Controllers that regulate the orientation of the torso have been formulated for passive walking machines [10, 11], partial gait models [12], and more recently a sagittal plane walking model [13]. Each of these models has its drawbacks when considered in the context of human walking: the passive walking machines display a lot of torso sway relative to a human [14]; the partial gait model [12] assumes that the hip torque applied to the torso does not change the force vector applied to the hip; and the sagittal plane walking model [13] uses a heuristic controller, which has unknown stability properties and exhibits more torso sway than a human does while walking [14].

Recently, Poulakakis and Grizzle [15, 16] used input-output feedback linearization to embed desirable torso dynamics into the controller of a simplified planar robot (Fig. 1B). Their model, the asymmetric spring loaded inverted pendulum (ASLIP), consists of a planar biped with massless, telescoping legs that attach at the hip joint of the torso. The center-of-mass (COM) of the torso is not coincident with the hip joint, adding non-trivial torso dynamics to the system equations of the biped. Poulakakis and Grizzle used the hip torque and leg force (the linear force generated by the telescoping leg) of the model to control the state of the torso. This control was achieved by embedding the dynamics of the desired plant (Fig. 1A), the spring loaded inverted pendulum (SLIP model), into the control laws for the hip torque and leg force of the ASLIP using input-output feedback linearization [17, 18].

Interestingly there is a high degree of similarity between human COM kinematics and ground reaction force profiles to those of the SLIP model during both walking and running [19]. The COM kinematics and ground reaction force profiles can be made to fit simultaneously within ±1 standard deviation of human profiles [14] if the point contacts of the SLIP model are allowed to translate forward at a velocity that is similar to the center-of-pressure (COP) velocity in humans [20]. The quality of fit between the SLIP model and human walking and the illustration that this gait can be embedded in more elaborate models [15, 16] inspired the current investigation to determine if human-like SLIP dynamics could be embedded into a sagittal plane human gait model. The investigation first begins by extending Poulakakis and Grizzle's ASLIP model and control laws to a bipedal ASLIP model in Sec. 2, simulates walking motions, and then proceeds to apply the same control framework to a multibody sagittal plane gait model in Sec. 3.

2. The SLIP and ASLIP models

The standard planar SLIP model (denoted with a subscript 'S' in equations) consists of a point mass (m) in a uniform gravity field, g, with two massless linear springs with a fixed resting length (r_0) and no preload (Fig. 1A). Each leg behaves like a massless prismatic joint (actuated by forces of magnitude $p_{S,1}$ and $p_{S,2}$) connected to the ground (during stance) with revolute joints. Together both legs exert a net force of f_{Sx} and f_{Sy} to the SLIP point mass in the horizontal x and vertical directions y respectively. Although the dynamic equations of the SLIP model, Eqns. 1-2 , are very simple, it can be made to walk or run with human-like ground reaction force and COM kinematic profiles [19] using optimized initial conditions selected to yield limit-cycle walking or running.

$$\ddot{x}_S = \frac{1}{m} f_{Sx} \tag{1}$$

$$\ddot{y}_S = \frac{1}{m}(f_{Sy} - mg) \tag{2}$$

The legs of the SLIP behave like linear springs attached to the ground through a revolute joint at point $(cx_i, cy_i$, where $i = 1$ for leg 1, and $i = 2$ for leg 2) until the foot leaves the ground (when $r_0 + \frac{y_S}{\sin(\alpha_{S,i})} < 0$, note $\alpha_{S,i}$ is negative) putting the leg into swing. The swing limb is held at a constant angle ϕ_S (its terminal swing angle) relative to the stance limb until the foot contacts the ground (when $r_0 + \frac{y_S}{\sin(\alpha_{S,i})} \geq 0$). The swing limb angle was defined with respect to the stance limb, rather than the inertial frame [19], because this definition appears to offer increased orbital stability for slow walking gaits. It is assumed that the spring freely rotates about both the mass and the ground during stance, and that the contact end of the spring sticks and does not slip.

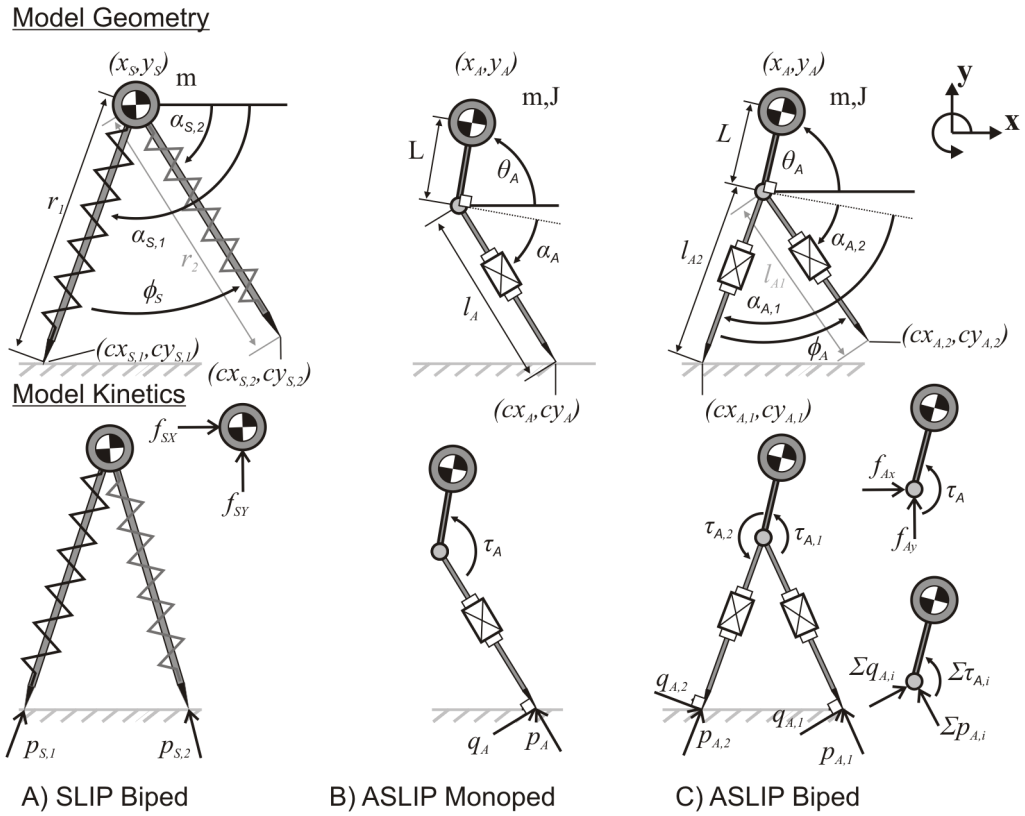

Fig. 1: The bipedal SLIP model is shown in panel A). The monopedal ASLIP [15] is shown in panel B). The bipedal ASLIP developed in this work is in panel C). The sign of each angle and torque follows the right hand rule

The net force acting on the point mass, (f_{Sx}, f_{Sy}), can be found using Eqns. 4 and 5 as the sum of the spring forces generated by each leg defined in Eqn. 3. The variable n is used throughout the equations in this paper to denote the number of legs in contact with the ground; n is set to 1 for single stance, and 2 for double stance.

$$p_{S,i} = -k_i(r_i - r_0) \tag{3}$$

$$f_{Sx} = \sum_{i=1}^{n} -p_{S,i}\cos(\alpha_{S,i}) \tag{4}$$

$$f_{Sy} = \sum_{i=1}^{n} -p_{S,i}\sin(\alpha_{S,i}) \tag{5}$$

Substituting in Eqns. 3-5 into Eqns. 1-2 yields the dynamic equations of motion for a monopedal SLIP (n set to 1) and

the bipedal SLIP (n set to 2) during stance.

$$\ddot{x}_S = \frac{1}{m}\sum_{i=1}^{n} k_i(r_i - r_0)\cos(\alpha_{S,i}) \tag{6}$$

$$\ddot{y}_S = \frac{1}{m}\left(\sum_{i=1}^{n} k_i(r_i - r_0)\sin(\alpha_{S,i}) - mg\right) \tag{7}$$

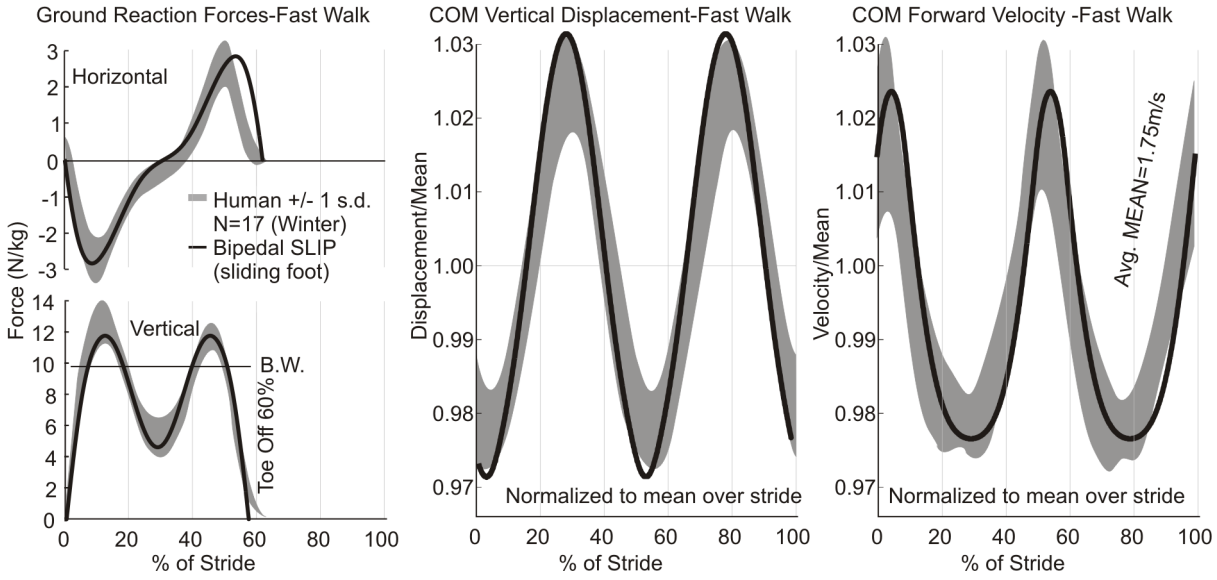

Fig. 2: A comparison of the COM kinematics and ground reaction forces generated by a bipedal sliding SLIP model (black) and human curves (gray) [14] during a single gait cycle at a fast pace

The ground reaction force profiles and COM kinematics of human gait and the gait of the SLIP model can be very similar [19], which suggests that humans control their legs to act like linear springs during steady state walking and running. The similarity can be further improved if the contact point is translating forward (a sliding SLIP model) at a constant velocity that is matched to the average center of pressure velocity of human running [20]. The walking motion of a bipedal SLIP model was simulated (Fig. 2) using Eqns. 6-7 to compare the COM kinematics and ground reaction force profiles of the model to human data [14]. The parameters chosen for the model was consistent with Geyer et al.'s SLIP simulation [19] — with an $1.80\,m$ tall, $80\,kg$ man walking at $1.75\,m/s$ — except the contact point translated horizontally with a velocity of $0.25\,m/s$, approximating the average COP translation of a human during walking. The mass of the SLIP model represents the mass of the head, arms and trunk (in this case $m = 54.2\,kg$) calculated using anthropometric tables [1]. The legs of the bipedal SLIP model had a stiffness of $13\,kN/m$ and were held at $\phi_S = 0.6$ radians apart during swing to maintain a stable limit cycle at this quick walking speed. The stiffness of the legs was chosen to be consistent with the frequency constant ($f = \sqrt{k/m}$) of Geyer et al.'s SLIP simulation [19].

The SLIP model can be made to resemble the human form more closely by adding a hip joint and a torso above the massless legs. Poulakakis and Grizzle introduced an asymmetric monopedal (running) SLIP model (ASLIP, denoted with a subscript 'A') that included a torso, with the linear leg actuators terminating at a hip joint (Fig. 1B). The equations of motion of the ASLIP, Eqns. 8-10, are very similar to those of the SLIP but include torso (of mass m, inertia J, length L, oriented at angle θ_A relative to the inertial frame) dynamics, which are a critical component for an

anthropomorphic gait model.

$$\ddot{x}_A = \frac{1}{m} f_{Ax} \tag{8}$$

$$\ddot{y}_A = \frac{1}{m}(f_{Ay} - mg) \tag{9}$$

$$\ddot{\theta}_A = \frac{1}{J}(L(f_{Ax}\sin(\theta_A) - f_{Ay}\cos(\theta_A)) + \tau_A) \tag{10}$$

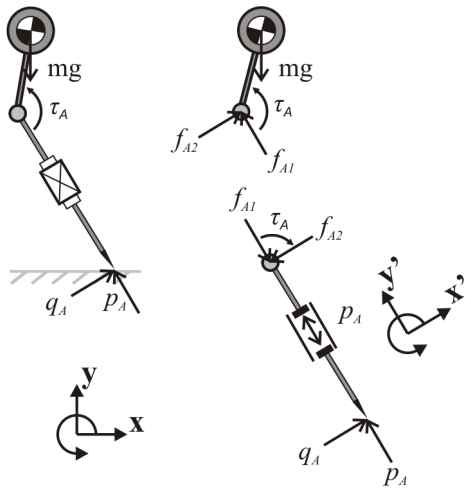

Fig. 3: Free body diagram of the ASLIP. The leg has been drawn to emphasize that it behaves like a massless telescoping force actuator

A statics analysis (Fig. 3) of the massless leg can be used to obtain the expressions for the forces and torques applied to the torso. In the local (x', y') axis parallel to the leg, with unit vectors $((\hat{x}', \hat{y}'))$, we have

$$\sum F \cdot \hat{x}' = 0,\ q_A - f_{A2} = 0 \tag{11}$$

$$\sum F \cdot \hat{y}' = 0,\ p_A - f_{A1} = 0 \tag{12}$$

$$\sum \tau = 0,\ -\tau_A + q_A l_A = 0. \tag{13}$$

Solving Eqns. 11-13 for the net force applied to the torso ($f_{A2}\hat{x}' + f_{A1}\hat{y}'$) as a function of the actuator outputs (p_A and τ_A), and resolving the result into the global coordinate frame yields

$$f_{Ax} = \sum_{i=1}^{n} -p_{A,i}\sin(\theta_A + \alpha_{A,i}) + \frac{\tau_{A,i}}{l_{A,i}}\cos(\theta_A + \alpha_{A,i}) \tag{14}$$

$$f_{Ay} = \sum_{i=1}^{n} p_{A,i}\cos(\theta_A + \alpha_{A,i}) + \frac{\tau_{A,i}}{l_{A,i}}\sin(\theta_A + \alpha_{A,i}). \tag{15}$$

The forces applied to the hip (horizontal f_{Ax} and vertical f_{Ay} forces) are no longer simply spring forces, but are the sum of the forces generated by the linear actuator $p_{A,i}$, and the reaction force $q_{A,i}$ created by the applied hip torque τ_A, as shown in Eqns. 14-15. Substituting Eqns. 14-15 into Eqns. 8-10 gives the equations of motion of the ASLIP during single stance (n=1) and double stance (n=2) phases. Note that since Poulakakis and Grizzle's ASLIP model is

monopedal, it only makes use of the single stance ($n = 1$) phase.

$$\ddot{x}_A = \frac{1}{m}\sum_{i=1}^{n}\left(-p_{A,i}\sin(\theta_A + \alpha_{A,i}) + \frac{\tau_{A,i}\cos(\theta_A + \alpha_{A,i})}{l_{A,i}}\right) \tag{16}$$

$$\ddot{y}_A = \frac{1}{m}\sum_{i=1}^{n}\left(p_{A,i}\cos(\theta_A + \alpha_{A,i}) + \frac{\tau_{A,i}\sin(\theta_A + \alpha_{A,i})}{l_{A,i}}\right) - g \tag{17}$$

$$\ddot{\theta}_A = \frac{1}{J}\sum_{i=1}^{n}\left(\tau_{A,i}\frac{l_{A,i} - L\sin(\alpha_{A,i})}{l_{A,i}} - Lp_{A,i}\cos(\alpha_{A,i})\right) \tag{18}$$

2.1. ASLIP Single Stance Phase Control

The ASLIP is able to run exactly like a SLIP model using the control laws that Poulakakis and Grizzle formulated that embed the dynamics of the SLIP model into the closed-loop equations of the ASLIP. They chose the hip torque, τ_A (where subscript 'A' denotes the ASLIP), to regulate the orientation of the torso of their single stance model using input-output feedback linearization [17, 18]. This control law can be found by setting the angular acceleration of the torso to an error term ν_θ, as shown in Eqn. 19, and solving for τ_A as in Eqn. 21.

$$\ddot{\theta}_A = \nu_\theta \tag{19}$$

Poulakakis and Grizzle formulated the feedback error term,ν_θ, for single stance, to render the desired orientation of the torso, θ_0, to an exponentially stable set point.

$$\nu_\theta = -K_\theta(\theta_A - \theta_0) - D_\theta\dot{\theta}_A \tag{20}$$

The hip torque that regulates the orientation of the torso to the error term, ν_θ, can be found by substituting Eqn. 19 into Eqn. 10 and solving for τ_A.

$$\tau_A = \nu_\theta J - L(f_{Ax}\sin(\theta_A) - f_{Ay}\cos(\theta_A)) \tag{21}$$

After substituting in Eqns. 14-15 for the single stance phase, Eqn. 21 becomes

$$\tau_A = l_A\frac{\nu_\theta J + Lp_A\cos(\alpha_A)}{l_A - L\sin(\alpha_A)}. \tag{22}$$

where all of the above subscript A terms refer to quantities associated with the monopedal — equivalent to single stance because the model has massless legs — ASLIP model (Fig. 1 B). After performing a coordinate transformation, Poulakakis and Grizzle arrived at a control law for the leg force, p_A, that renders the dynamic equations of the ASLIP identical to the SLIP when $\nu_\theta = 0$.

$$p_A = \frac{l_A - L\sin(\alpha_A)}{r_A}p_S \tag{23}$$

The nonlinear coordinate transformation required to derive Eqn. 23 is quite involved because both the SLIP and ASLIP models are underactuated (they have fewer actuators than degrees of freedom). Refer to Poulakakis's thesis [21] and Ch. 4 of Isidori [17] for details. Substituting Eqns. 22 and 23 into Eqns. 14-15 and finally into Eqns. 8-10 for the single stance phase case ($n = 1$) results in the closed-loop equations of motion for the monopedal ASLIP model.

$$\ddot{x}_A = \frac{(l_A - L\sin(\alpha_A))(l_A\sin(\theta_A + \alpha_A) - L\cos(\theta_A))\frac{p_S}{r} - \cos(\theta_A + \alpha_A)\nu_\theta J}{m(L\sin(\alpha_A) - l_A)} \tag{24}$$

$$\ddot{y}_A = \frac{(l_A - L\sin(\alpha_A))(-l_A\cos(\theta_A + \alpha_A) - L\sin(\theta_A))\frac{p_S}{r}}{m(L\sin(\alpha_A) - l_A)} + \frac{mg(l_A - L\sin(\alpha_A)) - \nu_\theta J\sin(\theta_A + \alpha_A)}{m(L\sin(\alpha_A) - l_A)} \tag{25}$$

$$\ddot{\theta}_A = \nu_\theta \tag{26}$$

After making use of a trigonometric identity (detailed in Poulakakis thesis [21]), the closed loop ASLIP equations become identical to the dynamic equations of the SLIP (Eqns. 6 and 7) but only when the torso of the ASLIP is being perfectly regulated ($\nu_\theta = 0$). The ASLIP and SLIP COM accelerations will differ when the torso of the ASLIP is not at the desired set point ($\nu_\theta \neq 0$ because $\theta_A \neq \theta_0$ and/or $\dot{\theta}_A \neq 0$) due to the extra hip torque that is required to regulate the orientation of the torso to the desired set point.

2.2. ASLIP Double Stance Phase Control

Here we extend Poulakakis and Grizzle's single stance ASLIP controller to function during double stance. The bipedal ASLIP and SLIP models both have a single stance phase as before, but now they also have a double stance phase which is necessary to simulate walking. In order to emulate the SLIP model during double stance, a control law must be derived that renders the closed loop bipedal ASLIP dynamic equations identical to the dynamic equations of the SLIP model.

$$\ddot{x}_A = \ddot{x}_S \tag{27}$$

$$\ddot{y}_A = \ddot{y}_S \tag{28}$$

$$\ddot{\theta}_A = \nu_\theta \tag{29}$$

The expression for the two hip torques, $\tau_{A,1}$ and $\tau_{A,2}$, that satisfy Eqn. 29 can be found by setting $\ddot{\theta}_A = \nu_\theta$ in Eqn. 18 and solving for $\tau_{A,1}$ and $\tau_{A,2}$.

$$\sum_{i}^{2} \tau_{A,i} \left(\frac{l_{A,i} - L\sin(\alpha_{A,i})}{l_{A,i}} \right) = \nu_\theta J + \sum_{i=1}^{2} L p_{A,i} \cos(\alpha_{A,i}) \tag{30}$$

During double stance the ASLIP model is overactuated because Eqn. 30 shows that there are four control variables to solve for (two hip torques $\tau_{A,1}$, $\tau_{A,2}$ and two leg forces $p_{A,1}$, $p_{A,2}$) yet only three equations, Eqns. 27-29, that these leg forces and hip torques need to satisfy. Although there is no unique solution to this system of equations, it can be solved analytically if a fourth equation is introduced. Here we introduce a fourth equation that constrains the torque generated by each hip to be proportional to the vertical component of the ground reaction force beneath each corresponding telescoping leg ($f_{Ay,1}$ and $f_{Ay,2}$). A physical interpretation of this heuristic is that torque is shared between each hip according to how much traction is present under the respective foot, an important consideration given that hip torques will result in a relatively large horizontal ground reaction force at the feet. Note that Eqn. 31 is a convenient heuristic, as it is not presently known how humans share torque across their hips during double stance.

$$\frac{\tau_{A,1}}{f_{Ay,1}} - \frac{\tau_{A,2}}{f_{Ay,2}} = 0 \tag{31}$$

Since the four equations (Eqns. 27-31) are linear in the four unknowns of interest ($\tau_{A,1}$, $\tau_{A,2}$, $p_{A,1}$ and $p_{A,2}$), they can be solved symbolically (using Maple [22]). The solution yields expressions for the two hip torques ($\tau_{A,1}$ and $\tau_{A,2}$) and leg forces ($p_{A,1}$ and $p_{A,2}$) that when substituted into the dynamic equations of the ASLIP will regulate the orientation of the torso and cause the COM trajectory of the ASLIP and SLIP models to match. The solutions for the previously described leg forces and hip torques are not reproduced in this manuscript due to their unwieldy size (the final expressions span several pages). As a note, this system of four equations could also be solved numerically. The performance differences between the symbolic and numeric solutions is presently not known.

The bipedal ASLIP and a bipedal SLIP (Eqns. 1-2) models were simulated (using ode45 in Matlab Simulink [23]) for comparison purposes. The bipedal ASLIP was simulated by using Poulakakis and Grizzle's closed loop expressions Eqns. 24-26 during single stance, and then Eqns. 16-18 ($n = 2$) using the solutions to Eqns. 27- 31 for the hip torques ($\tau_{A,1}$,$\tau_{A,2}$) and leg forces ($p_{A,1}$, $p_{A,2}$) during double stance. The swing angle of the ASLIP model, $\phi_{A,SW}$, was set so that the contact points of both the SLIP and the ASLIP would coincide. The inertia of the ASLIP represents inertia of the head, arms and trunk of this person (in this case $J = 3.6\,kg\,m^2$) and was calculated using an anthropometric table [1]. The forward velocity of the models was set to $1.2\,m/s$, with a COP velocity of $0.20\,m/s$ to more closely match a natural walking pace [14]. The remaining simulation parameters are identical to the ones used

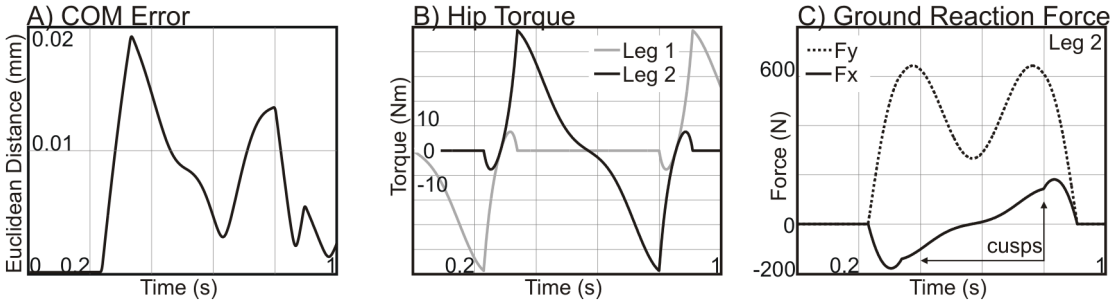

Fig. 4: Simulation results for a bipedal ASLIP model. The Euclidean distance between the bipedal ASLIP COM and SLIP COM is shown in panel A). The hip torques of the bipedal ASLIP during steady state walking are shown in panel B). The ground reaction forces generated by Leg 2 are shown in panel C)

to generate Fig. 2 as described in Sec. 2. The initial conditions of the model and the swing angle were selected using optimization (using fminsearch in Matlab) to yield a gait with a stable limit cycle.

The simulation results show that that there are subtle differences between the gait of the bipedal ASLIP and human gait. The ASLIP is able to regulate its torso far more accurately (within 2e-16 radians, of the desired orientation) than the $1^\circ - 2^\circ$ of torso sway that is typical of human gait [14] likely because its hip torques are not bandwidth limited, and its back segment is perfectly rigid. The sharp change in hip torque as the leg transitions from single to double stance (and vice versa) causes a subtle cusp in the horizontal ground reaction force profile (Fig. 4 C) that is not present in human ground reaction force profiles.

3. Mapping SLIP Torso Dynamics onto an Anthropomorphic Multibody Gait Model

An 11-dof anthropomorphic sagittal plane gait model (Fig. 5) was developed along with a control system for the legs to regulate the orientation of the torso of the multibody model and cause it to track the XY position of the target SLIP model. The multibody model is controlled using 6 joint torques applied at both hips, knees and ankles. The model interacts with the ground using a two-segment foot contact model — an extension of Millard et al. [24] — consisting of two spherical volumetric contact elements [25] to represent the heel and metatarsal pads. The midfoot is not rigid, but is allowed to flex slightly at a revolute joint that has a linear spring-damper in parallel with it.

Applying input-output feedback linearization to this model is particularly difficult due to the two-segment viscoelastic foot. Instead, an input-output feedback linearization control law is calculated for an approximate model (detailed in Sec. 3.1) which has a rigid foot. Since the control model is an approximation of the gait model, feedback control — supplied by the error terms (ν_x,ν_y and ν_θ) — is necessary to ensure that the orientation of the torso is regulated and its position converges with the COM location of the SLIP model.

$$\ddot{x}_M = \ddot{x}_S + \nu_x \tag{32}$$

$$\ddot{y}_M = \ddot{y}_S + \nu_y \tag{33}$$

$$\ddot{\theta}_M = \nu_\theta \tag{34}$$

Hip, knee and ankle torques that satisfy Eqns. 32-34 are computed for the multibody gait model using a series of control models (Fig. 6) that have a simplified foot, making it possible to use input-output feedback linearization [17, 18]. As with the ASLIP model, a set of additional heuristic equations are introduced during double stance to permit a unique set of joint torques to be computed to satisfy Eqns. 32-34 in this overactuated pose (here the torso has 3 dof, and there are 6 joint torques that can be applied).

Since the legs now have mass (in contrast to the previous models) a swing controller is required to guide the leg from its final push-off position to its contact position in a specific amount of time. The SLIP model is used to precompute the swing length Δ_X and time since only constant cadence walking is being considered. Guiding the leg from push-off to heel-contact in a set amount of time, in a manner that requires modest torque magnitudes, and keeps

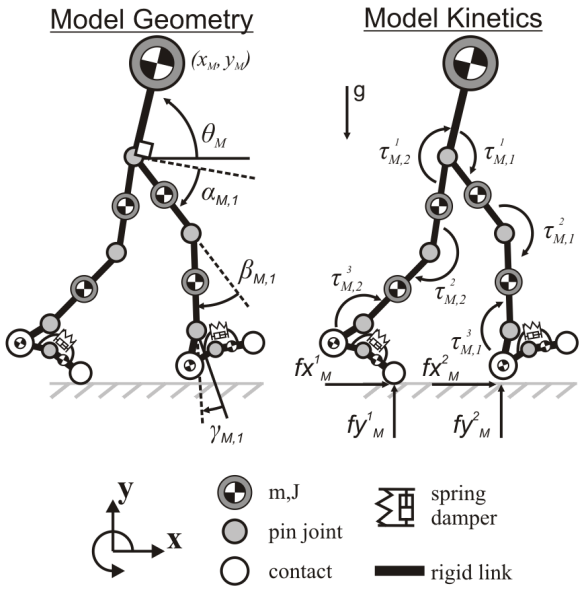

Fig. 5: The multibody model

the foot from scuffing the ground is a formidable two-point boundary value problem. Direct collocation optimization [26] was used to find a trajectory that satisfied these conditions. This pre-computed swing trajectory was used as a reference for a computed-torque controller to guide the swing limb on the multibody model. The following subsections detail the approach that was used to control the model during stance (Sec. 3.1) and swing (Sec. 3.3).

3.1. Single Stance Control

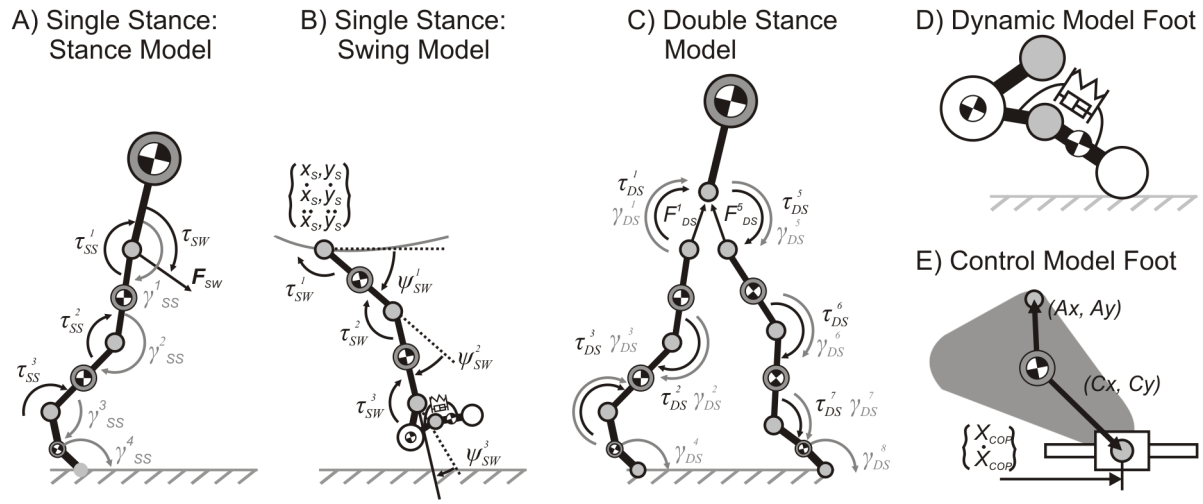

Fig. 6: The stance model A), the swing model B) and the double stance model C) used by the control system to compute the hip, knee and ankle torques. The actual foot contact model consists of a 2-part model that includes volumetric foot contact pads D), while the abstraction used by the control system treats the foot as a rigid link that rotates about a pin joint that is translating along a prismatic joint E)

While the importance of modeling the compliance of the human foot accurately has been noted by many in the gait modeling research community [8, 27, 28], a flexible and compliant foot complicates the control of the torso substantially. There is little information available in the literature on controlling bipeds that interact with the ground through a compliant foot. The compliance of the foot limits the forces that the leg can apply to the torso. Heel pad load cycles [29] suggest that human foot pads behave like nonlinear springs between the bones of the foot and the ground. When the foot pads are touching the ground, but have not reached steady state compression, the foot pads behave like a spring of low stiffness. The transient low stiffness of the foot pads greatly limits the ability of the leg to apply a desirable force and torque to the hip joint. As the pads of the foot compress, their apparent stiffness significantly increases and can be approximated as being rigid giving the leg greater control authority over the torso. While a compliant foot is used for the dynamic model (Fig. 6.D), a geometrically equivalent but rigid foot is used for the control model (Fig. 6.E).

During the transient contact phase when the apparent stiffness of the foot pads is quite low, the control model and the dynamic model differ. The two models are made to converge to one and other as the foot pads reach steady state compression by using feed-back control to augment the desired torso accelerations (Eqns. 32- 34). Each of the feedback error terms (ν_x,ν_y and ν_θ) take the form of a state feedback PD controller:

$$\nu_x = -K_x(x_M - x_S) - D_x(\dot{x}_M - \dot{x}_S) \tag{35}$$
$$\nu_y = -K_y(y_M - y_S) - D_y(\dot{y}_M - \dot{y}_S) \tag{36}$$
$$\nu_\theta = -K_\theta(\theta_M - \theta_0) - D_\theta(\dot{\theta}_M). \tag{37}$$

Input-output feedback linearization [17, 18] is used to compute the hip, knee, and ankle torques required to accelerate the torso of the multibody model such that Eqns. 32-34 are satisfied. The input-output feedback linearization control expressions are not formulated using the multibody model (Fig. 5) — due to the difficulties the full foot model introduces — but with an approximate single stance model (Fig. 6A) that includes a rigid foot. To form the control law, we first begin with the equations of motion of the stance control model (Fig. 6A) in functional form (using square brackets to denote matrices).

$$\ddot{\vec{\gamma}}_{SS} = [M_{SS}]^{-1}_{4\times4}\left(-\vec{C}_{SS} + [P_{SS}]_{4\times3}\{\vec{\tau}_{SS}\}_{3\times1} + [Q_{SS}]_{4\times3}\left\{\begin{array}{c}\vec{F}_{SW}\\ \vec{\tau}_{SW}\end{array}\right\}_{3\times1}\right) \tag{38}$$

In Eqn. 38 $\vec{\gamma}_{SS}$ is the vector of joint angles (and respective derivatives) of the single stance (SS) control model (Fig. 6A), $[M_{SS}]$ is the mass matrix, $\vec{C}_{SS}$ the vector of Coriolis, centripetal and gravitational forces; $[P_{SS}]_{4\times3}$ is the matrix that transforms the joint torques $\{\vec{\tau}_{SS}\}_{3\times1}$ into generalized forces; and $[Q_{SS}]_{4\times3}$ is the matrix that transforms the reaction force and torque vector $\left\{\vec{F}_{SW}, \vec{\tau}_{SW}\right\}_{3\times1}$ (that the swing limb applies to the pelvis) into generalized forces. The variables used to describe the general multibody terms in Eqn. 38 are used throughout this chapter. The accelerations of the torso $(\ddot{x}_M, \ddot{y}_M, \ddot{\theta}_M)$ can be expressed as a linear combination of the joint accelerations of the stance model. After substituting the Eqns. 32-33, the SLIP emulation equations, the mapping from the accelerations of the torso to the angular accelerations of the joints of the leg becomes:

$$\left\{\begin{array}{c}\ddot{x}_S + \nu_x\\ \ddot{y}_S + \nu_y\\ \ddot{\theta}_S + \nu_\theta\end{array}\right\} = [T_{SS}]_{3\times4}\left\{\ddot{\vec{\gamma}}_{SS}\right\}. \tag{39}$$

Substituting Eqn. 38 into Eqn. 39 yields a set of three equations that is linear in the three joint torques $\vec{\tau}_{SS}$.

$$\left\{\begin{array}{c}\ddot{x}_S + \nu_x\\ \ddot{y}_S + \nu_y\\ \ddot{\theta}_S + \nu_\theta\end{array}\right\} = [T_{SS}]_{3\times4}[M_{SS}]^{-1}_{4\times4}\left(-\vec{C}_{SS} + [P_{SS}]_{4\times3}\{\vec{\tau}_{SS}\}_{3\times1} + [Q_{SS}]_{4\times3}\left\{\begin{array}{c}\vec{F}_{SW}\\ \vec{\tau}_{SW}\end{array}\right\}_{3\times1}\right) \tag{40}$$

Once the state of the multibody model has been mapped to an equivalent state of the stance model, Eqn. 40 becomes a system of three equations with three unknowns (the three components of $\vec{\tau}_{SS}$) making it possible to compute values of the hip, knee and ankle torques that will satisfy Eqns. 32-34. The hip, knee and ankle states can be mapped directly from the multibody model to the stance control model.

$$\gamma^1_{SS} = -(\theta_M - \frac{\pi}{2} + \alpha_M) \quad (41)$$
$$\gamma^2_{SS} = -\beta_M \quad (42)$$
$$\gamma^3_{SS} = -\gamma_M \quad (43)$$
$$\dot{\gamma}^1_{SS} = -(\dot{\theta}_M + \dot{\alpha}_M) \quad (44)$$
$$\dot{\gamma}^2_{SS} = -\dot{\beta}_M \quad (45)$$
$$\dot{\gamma}^3_{SS} = -\dot{\gamma}_M \quad (46)$$

The geometry of the foot of the control model (Fig. 6A) — the length of the link between the COM of the foot and the revolute joint attached to the ground — is adjusted so that the revolute joint attaches to the ground at a location that coincides with the COP of the foot of the multibody model (Fig. 5). The angular velocity of the stance model foot, and the translational velocity of the COP of the stance model ($\dot{\gamma}^4_{SS}$ in Fig. 6A and $\dot{x}_{COP}$ in Fig. 6E) are computed such that the translational velocity of the ankle joints of the stance control and multibody gait model match.

3.2. Double Stance Control

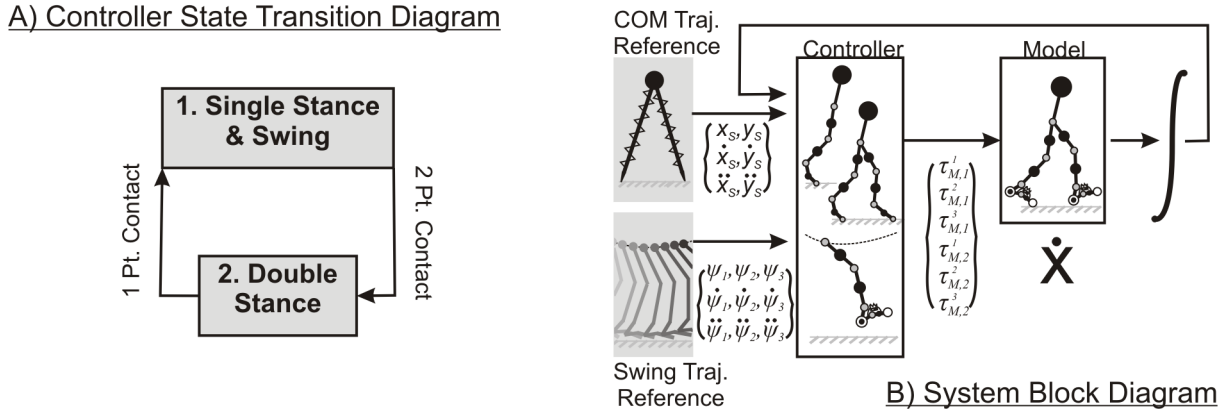

Fig. 7: The single and double stance control models are switched as a function of foot contact A). The gait model is controlled by the multibody swing and stance models which use the SLIP and swing reference kinematics as desirable trajectories B)

Once the swing foot comes into contact with the ground, the controller changes its internal state from single stance to double stance (Fig. 7), and employs a completely different control model (Fig. 6C), for which a new control law must be derived. As before, input-output feedback linearization is applied to an approximate double stance model to yield hip, knee and ankle torques for both legs that will satisfy Eqns. 32-34. The derivation begins by computing the net force and torque that the two legs must apply to the torso to satisfy Eqns. 32-34.

$$f_{Mx} = m(\ddot{x}_M + \nu_x) \quad (47)$$
$$f_{My} = m(\ddot{y}_M + \nu_y + g) \quad (48)$$
$$\tau_M = J\nu_\theta - L(f_{Mx}\sin(\theta_M) - f_{My}\cos(\theta_M)) \quad (49)$$

Scalars f_{Mx},f_{My}, and τ_M are the net force and torque that the two legs must apply to the torso (of mass m, inertia J at an orientation of θ_M as before) to satisfy Eqns. 32-34. The net force and torque applied to the torso is simply the sum of the force and torque that each leg applies to the hip joint. As before, horizontal and vertical unit vectors $(\hat{x}, \hat{y})$ are indicated with a circumflex.

$$f_{Mx} = (\vec{F}^1_{DS} + \vec{F}^5_{DS}) \cdot \hat{x} \quad (50)$$

$$f_{My} = (\vec{F}^1_{DS} + \vec{F}^5_{DS}) \cdot \hat{y} \quad (51)$$

$$\tau_M = \tau^1_{DS} + \tau^5_{DS} \quad (52)$$

Since the net force and torque that is applied to the torso is only comprised of three variables, yet is a function of six joint torques (τ^{1-3}_{DS} and τ^{5-7}_{DS}), there is no unique solution to this system of equations. As before with the ASLIP model, extra heuristic equations are introduced to divide the load between the two legs in proportion to the contact force beneath the respective foot of the multibody model.

$$\frac{\vec{F}^1_{DS} \cdot \hat{x}}{fy^1_M} + \frac{\vec{F}^5_{DS} \cdot \hat{x}}{fy^2_M} = 0 \quad (53)$$

$$\frac{\vec{F}^1_{DS} \cdot \hat{y}}{fy^1_M} - \frac{\vec{F}^5_{DS} \cdot \hat{y}}{fy^2_M} = 0 \quad (54)$$

$$\frac{\tau^1_{DS}}{fy^1_M} - \frac{\tau^5_{DS}}{fy^2_M} = 0 \quad (55)$$

The system of six equations (Eqns. 50-52 and Eqns. 53-55) can be solved for the forces and torques that each leg must apply to hip joint of the torso to satisfy Eqns. 47-49 and Eqns. 50-52. The force and torque that each leg applies to the hip joint of the torso can be used in combination with the equations of motion of the double stance model (Fig. 6C) to compute the remaining knee and ankle torques that each leg must generate. The equations of motion of the double stance model in functional form are

$$[M_{DS}]_{9\times9}\left\{\ddot{\vec{\gamma}}_{DS}\right\} + \vec{C}_{DS} + \left\{ \begin{array}{c} 0_{5\times1} \\ \vec{D}_{DS,4\times1}\vec{\lambda} \end{array} \right\} = [P_{DS}]_{9\times6}\left\{\vec{\tau}_{DS}\right\}_{6\times1}. \quad (56)$$

Position constraint equations $\vec{D}_{DS}$ have been used to model the hip joints (rather than using joint coordinates) to make it possible to solve for the force that the legs apply at this joint. The reaction force at the hip can now be expressed as

$$\left\{ \begin{array}{c} \vec{F}^1_{DS} \\ \vec{F}^5_{DS} \end{array} \right\}_{4\times1} = [B_{DS}]_{4\times4}\left\{\vec{\lambda}\right\} \quad (57)$$

where matrix $[B_{DS}]_{4\times4}$ is a matrix that transform the Lagrange multipliers into reaction forces. After solving Eqn. 57 for the Lagrange multipliers that yield the desired joint reaction forces and substituting the result into Eqn. 56 we have

$$[M_{DS}]_{9\times9}\left\{\ddot{\vec{\gamma}}_{DS}\right\} + \vec{C}_{DS} + \left\{ \begin{array}{c} 0_{5\times1} \\ \vec{D}_{DS,4\times1}[B_{DS}]^{-1}\left\{ \begin{array}{c} \vec{F}^1_{DS} \\ \vec{F}^5_{DS} \end{array} \right\}_{4\times1} \end{array} \right\} = [P_{DS}]_{9\times6}\left\{\vec{\tau}_{DS}\right\}_{6\times1} \quad (58)$$

Since the two hip torques (τ^1_{DS} and τ^5_{DS}) and forces (f^1_{DS} and f^5_{DS}) are known from the solution to Eqns. 50-52 and Eqns. 53-55, Eqn. 58 has embedded in it a set of four equations (the constraint equations) that are linear in four unknowns (τ^2_{DS}, τ^3_{DS}, τ^6_{DS}, and τ^7_{DS}). After the state of the multibody model (Fig. 5) is mapped to the equivalent state of the double stance control model (Fig. 6) — using the same procedure detailed in Sec. 3.1 — Eqn. 57 can be solved for the remaining knee and ankle torques required to satisfy Eqns. 47-49.

3.3. Swing Control

The swing phase has been a topic of robotics research for many years and has resulted in a number of standard approaches: active trajectory tracking [4, 30], passive swing [11, 31], and a combination of passive and active swing techniques [32]. Although a lot of research has been done on the topic of swing, little of it is directly applicable to

formulating a control law that will yield a human-like swing phase. A purely passive swing is quite limiting because the swing frequency of the limb is fixed by the geometrical and inertial properties of the limb. In addition, it has been shown that a purely passive swing is incompatible with the human swing phase [33]. A purely trajectory driven approach is convenient, however, great care must be taken to choose a trajectory that does not require joint torques that would be impossible for a human to generate. Beginning the swing phase passively and finishing with trajectory tracking [32] seems like a logical approach, though care must be taken to blend the two phases in a manner that does not cause torque transients.

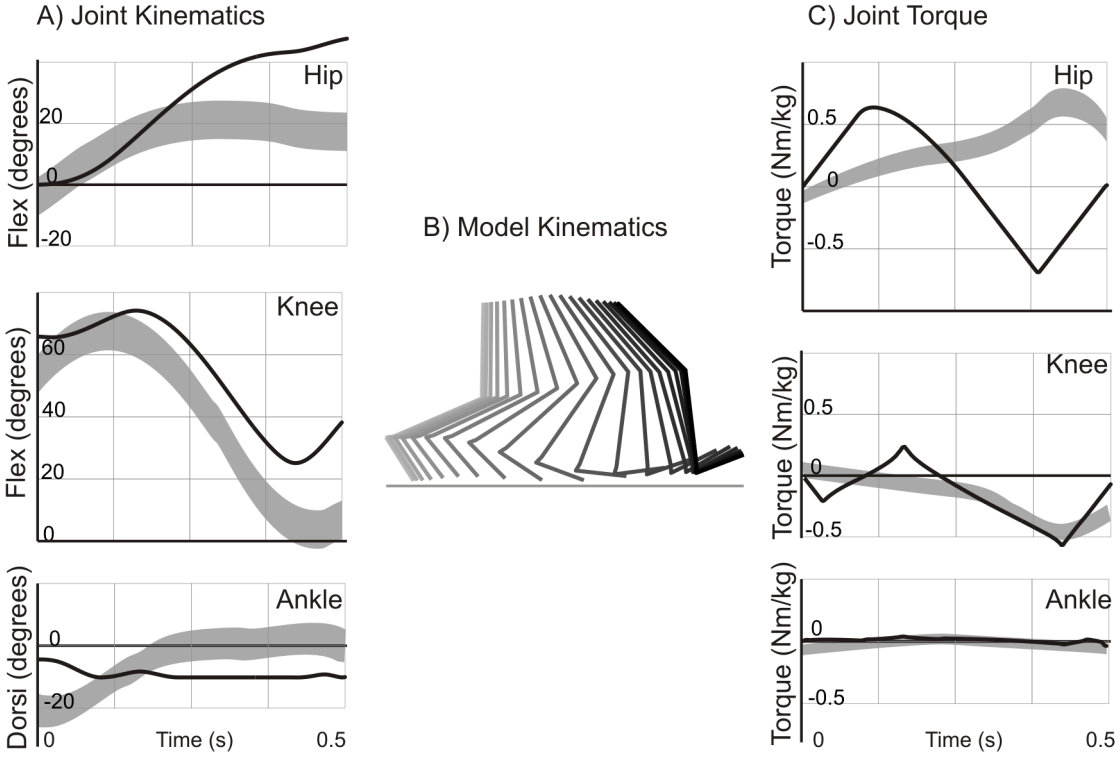

Fig. 8: Swing phase simulation results. Model and human joint kinematics (in gray) are shown in A), a stick figure diagram is presented in B) and plots of model and human normalized joint torques (in gray) are shown in C). Human data [14] is presented as a gray band that encompasses ±1 s.d.

For this preliminary investigation, optimization was used to pre-compute a human-like swing trajectory. During the multibody simulation, the swing limb was driven to follow the pre-computed optimal swing trajectory using a computed torque controller with feedback. Human-like swing kinematics that fit the swing phase of the target SLIP model were found by searching for a trajectory that minimized a convex function of joint work for the swing model (Fig. 6B). A convex function of joint work was employed to crudely emulate the increased metabolic cost of eccentric and concentric contractions relative to isometric contractions [34]. Note that the joint angles of the swing model are represented using the variables $\psi^1_{SW}, \psi^2_{SW}, \psi^3_{SW}$ in the place of α_M, β_M and γ_M for convenience.

$$min \sum_{i=1}^{3} \int_{t0}^{tf} (\tau^i_{SW} \dot{\psi}^i_{SW})^2 dt \tag{59}$$

Unlike the stance model, bandwidth-limited joint torque actuators were used during the optimization process. It was critical to use bandwidth-limited joint torque actuators to prevent the optimization algorithm from converging on a solution that required sharp changes of joint torque outside of human capabilities. Each torque actuator was modeled

as having a second-order, critically damped ($\zeta = 1$, $\omega_N = 8Hz \times 2\pi\, rad$) impulse response to a torque demand μ^i to crudely approximate the behavior of an equivalent set of muscles [1].

$$\ddot{\tau}^i = \omega_N^2 \mu^i - 2\zeta\omega_N \dot{\tau}^i - \omega_N \tau^i \tag{60}$$

Direct collocation [26] was used to solve this constrained problem to find solutions that satisfied the equations of motion,

$$[M_{SW}]_{3\times3} \left\{ \ddot{\vec{\psi}}_{SW} \right\} + \vec{C}_{SW} = [P_{SW}]_{3\times3} \left\{ \vec{\tau}_{SW} \right\}_{3\times1} \tag{61}$$

prevented the heel and toe from touching the ground during the swing period,

$$\left\{ \begin{array}{c} y_{HEEL} \\ y_{TOE} \end{array} \right\} > 0 \tag{62}$$

and finished with the heel at the desired contact location, Δ_x, as defined by the target SLIP model,

$$\left\{ \begin{array}{c} x_{HEEL} \\ y_{HEEL} \end{array} \right\} = \left\{ \begin{array}{c} \Delta_X \\ 0 \end{array} \right\}. \tag{63}$$

The accelerations of the hip, required in Eqn. 61, were set to the vertical and horizontal accelerations of the SLIP model. The kinematics and torques of the minimal joint work swing trajectory reveal significant differences from human swing (Fig. 8). Although the hip and knee initial positions are very similar, the final position of the model requires more flexion at the hip and knee than is typical of a human swing [14]. The hip torque of the model is markedly different from human hip torques [14] (estimated using inverse dynamics analysis), taking on a sinusoidal form. These differences are likely due to both model differences — none of the passive muscle properties are being modeled — and cost function differences. For the present study this plausible, but clearly un-human swing trajectory will be used to guide the swing leg to its final position at heel contact.

Once the swing trajectory was established, the swing limb was controlled to follow this trajectory using a standard computed torque controller [35] as shown in Eqn. 64.

$$\{\vec{\tau}_{SW}\}_{3\times1} = [P_{SW}]^{-1}_{3\times3} \left([M_{SW}]_{3\times3} \left\{ \ddot{\vec{\psi}}^*_{SW} \right\} + \vec{C}_{SW} \right) \tag{64}$$

Since the actual hip acceleration of the multibody model may differ from the desired vertical and horizontal accelerations of the target SLIP model, the state feedback controller shown in Eqn. 65 was used to ensure that the swing limb would converge to its desired trajectory over time.

$$\left\{ \begin{array}{c} \ddot{\psi}^{*1}_{SW} \\ \ddot{\psi}^{*2}_{SW} \\ \ddot{\psi}^{*3}_{SW} \end{array} \right\} = \left\{ \begin{array}{c} \ddot{\psi}^{1}_{SW} \\ \ddot{\psi}^{2}_{SW} \\ \ddot{\psi}^{3}_{SW} \end{array} \right\} - K_{SW} \left\{ \begin{array}{c} \alpha_M - \psi^1_{SW} \\ \beta_M - \psi^2_{SW} \\ \gamma_M - \psi^3_{SW} \end{array} \right\} - D_{SW} \left\{ \begin{array}{c} \dot{\alpha}_M - \dot{\psi}^1_{SW} \\ \dot{\beta}_M - \dot{\psi}^2_{SW} \\ \dot{\gamma}_M - \dot{\psi}^3_{SW} \end{array} \right\} \tag{65}$$

4. Multibody Control Mapping Evaluation via Simulation

The multibody model and control system was numerically simulated. At each timestep Eqns. 64 and 65 were used to apply torques to the hip, knee and ankle of the swing limb to ensure that it tracked the desired swing trajectory. The reaction force and torque, F_{SW} and τ_{SW}, that the swing limb applied to the hip joint, along with the desired torso accelerations from Eqns. 32-34 were substituted into Eqn. 40 prior to solving for the stance limb control torques τ^1_{SS}, τ^2_{SS} and τ^3_{SS} during single stance; and Eqn. 58 during double stance.

The simulation results (Fig. 9) indicate that the swing and stance controllers performed well, but problems were encountered during the transition between these phases (as the spurious ground reaction force in Fig. 9C displays). The stance controller limited the (Euclidean) distance error between the torso of the multibody model and the SLIP reference model to less than 1mm, though relatively high levels of feedback were required ($K_x = K_y = D_x = D_y = 10^3$ $\frac{N}{m}$ and $\frac{Ns}{m}$ respectively;$K_\theta = D_\theta = 10^4$ $\frac{Nm}{rad}$ and $\frac{Nms}{rad}$ respectively, each set by hand tuning) to make the SLIP and the multibody torso trajectories converge. During this time, the stance foot moved from being flat on the ground to rotating

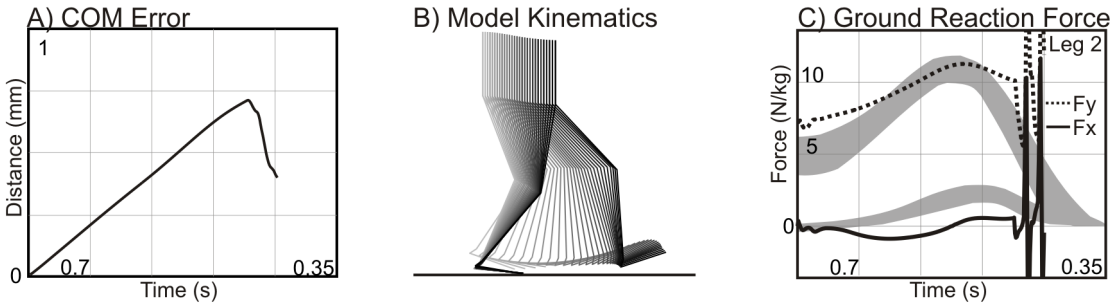

Fig. 9: Multibody gait simulation results. SLIP tracking works very well during single stance but fails at the end of swing

about the toe smoothly. When the swing limb reached its final posture, the target accelerations $\ddot{\psi}^i_{M,W}$ and velocities $\dot{\psi}^i_{M,W}$ were set to zero. This sudden change in desired acceleration and velocity caused the swing controller of Eqn. 64 to apply large torques to the swing limb. These large control torques resulted in correspondingly large reaction forces at the hip joint, causing the stance controller to go unstable (Fig. 9). Double stance was never reached.

The failure of this control system highlights a fundamental challenge of controlling the state of the torso during stance, and then controlling the state of the leg during swing: blending these two different control paradigms smoothly is difficult. Since the state of the leg is not controlled during stance (the state of the torso is), the posture of the leg at the end of stance is not known a priori. The state feedback terms (Eqn. 65) in the present swing controller (Eqn. 64) compute large control torques because the state of the leg was different from the pre-computed swing trajectory. It is likely that similar spurious control torques would be observed during the transition from stance to swing.

5. Conclusions

Although SLIP models have human-like running and walking gaits, it is challenging to map this behavior to an anthropomorphic model. A bipedal extension of Poulakakis and Grizzle's ASLIP monopedal model and control laws was presented. The presented control laws for the bipedal ASLIP make its state equations identical to the bipedal SLIP model. Mapping the torso dynamics of the SLIP model onto the joint torque space of a full multibody sagittal plane model with simulated foot contact proved challenging. Although a new stance controller formulation was developed, the transition from swing to stance (and likely vice-versa) resulted in large control torques, eventually causing the model to fall.

6. Future Work

Future work should concentrate on determining how best to coordinate the legs during double stance, and on developing controllers that allow the multibody model to emulate the SLIP while ensuring smooth transitions stance to swing. The spurious transitions between swing and stance phases of the multibody model could likely be smoothed if the SLIP target model has continuous swing and stance phases. Such a model could be employed to generate not only human-like torso trajectories, but also smooth human-like foot trajectories during swing and stance. Future work is going to concentrate on developing a simple model that has efficient equations of motion — to increase the number of gaits that can be tested using optimization — and exhibits human-like COM kinematic, ground reaction force, and swing limb profiles.

Acknowledgments

This research was supported by the Natural Sciences and Engineering Research Council of Canada.

References

[1] D. Winter, Biomechanics and Motor Control of Human Movement, 3rd Edition, John Wiley and Sons, Hoboken, NJ, 2005.
[2] S. Delp, J. Loan, M. Hoy, F. Zajac, E. Topp, J. Rosen, An interactive graphics-based model of the lower extremity to study orthopaedic surgical procedures, IEEE Transactions on Biomedical Engineering 37 (8) (1990) 757–767.
[3] J. Grizzle, G. Abba, F. Plestan, Asymptotically stable walking for biped robots: Analysis via systems with impulse effects, IEEE Transactions on Automatic Control 46 (1) (2001) 51–64.
[4] E. Westervelt, J. Grizzle, C. Chevallereau, J. Choi, B. Morris, Feedback Control of Dynamic Bipedal Robot Locomotion, CRC Press, 2007.
[5] S. Srinivasan, I. Raptis, E. Westervelt, Low-dimensional sagittal plane model of normal human walking, ASME Journal of Biomechanical Engineering 130 (2008) 051017–1 — 051017–11.
[6] G. Taga, A model of the neuro-musculo-skeletal system for human locomotion, Biological Cybernetics 73 (1995) 97–111.
[7] M. Wojtyra, Multibody simulation model of human walking, Mechanics Based Design of Structures and Machines 31 (3) (2003) 357–377.
[8] M. Millard, J. McPhee, E. Kubica, Multi-step forward dynamic gait simulation, in: C. Bottasso (Ed.), Multibody Dynamics: Computational Methods and Applications, Springer, 2009, pp. 25–43.
[9] M. Peasgood, E. Kubica, J. McPhee, Stabilization and energy optimization of a dynamic walking gait simulation, ASME Journal of Computational and Nonlinear Dynamics 2 (2007) 65–72.
[10] T. McGeer, Dynamics and control of bipedal locomotion, Journal of Theoretical Biology 163 (1993) 277–314.
[11] M. Wisse, D. Hobbelen, A. Schwab, Adding an upper body to passive dynamic walking robots by means of a bisecting hip mechanism, IEEE Transactions on Robotics 23 (2007) 112–123.
[12] E. Kubica, D. Wang, D. Winter, Feedforward and deterministic fuzzy control of balance and posture during human gait, in: Proceedings of the 2001 IEEE International Conference on Robotics and Automation, 2001, pp. 372–380, Seoul, Korea.
[13] H. Geyer, H. Herr, A muscle reflex model that encodes principles of legged mechanics produces human walking dynamics and muscle activities, IEEE Transactions on Neural Systems and Rehabilitation Engineering 18 (2010) 263–273.
[14] D. Winter, Biomechanics and Motor Control of Human Gait: Normal, Elderly and Pathological, 2nd Edition, University of Waterloo Press, 1991.
[15] I. Poulakakis, J. Grizzle, Formal embedding of the spring loaded interved pendulum in an asymmetric hopper, in: Proc. of the European Control Conference, 2007, pp. 1–8, Kos, Greece.
[16] I. Poulakakis, J. Grizzle, Monopedal running control: Slip embedding and virtual constraint controllers, in: Proc. of the IEEE/RSJ International Conference of Intelligent Robots and Systems, 2007, pp. 323–330, San Diego, California.
[17] A. Isidori, Nonlinear Control Systems Systems, 3rd Edition, Springer, New Jersey, 1995.
[18] H. Khallil, Nonlinear Systems, 3rd Edition, Prentice Hall, New Jersey, 2001.
[19] H. Geyer, A. Seyfarth, R. Blickhan, Compliant leg behaviour explains basic dynamics of walking and running, Proeedings of The Royal Society B 276 (2006) 2861–2867.
[20] S. Bullimore, J. Burn, Consequences of forward translation of the point of force application for the mechanics of running, Journal of Theoretical Biology 238 (2006) 211–219.
[21] I. Poulakakis, Stabilizing monopedal robot running: Reduction-by-feedback and compliant hybrid zero dynamics, Ph.D. thesis, The University of Michigan (December 2009).
[22] MapleSoft, Maplesim online documentation, http://www.maplesoft.com.
[23] MathWorks, Matlab online documentation, http://www.mathworks.com.
[24] M. Millard, J. McPhee, E. Kubica, Multi-step forward dynamic gait simulation, in: Proceedings of the Multibody Dynamics 2007, ECCOMAS Thematic Conference, 2007, pp. 1–17, Milano, Italy.
[25] Y. Gonthier, J. McPhee, C. Lange, J. Piedboeuf, A contact modeling method based on volumetric properties, in: Proceedings of the 5th International Conference on Multibody Systems, Nonlinear Dynamics and Control, 2005, pp. 477–486.
[26] A. Rao, D. Benson, C. Darby, M. Patterson, C. Francolin, I. Sanders, G. Huntington, Algorithm 902: GPOPS, a matlab software for solving multiple-phase optimal control problems using the gauss pseudospectral method, ACM Trans. Math. Softw. 37 (2) (2010) 1–39.
[27] F. Anderson, M. Pandy, Dynamic optimization of human walking, Journal of Biomechanical Engineering 123 (2001) 381–390.
[28] M. Ackermann, W. Schiehlen, Dynamic analysis of human gait disorder and metabolic cost estimation, Archive of Applied Mechanics 75 (2006) 569–594.
[29] P. Aerts, R. Kerr, D. de Clercq, D. Ilsley, R. Alexander, The mechanical properties of the human heel pad: a paradox resolved, Journal of Biomechanics 28 (1995) 1299–1308.
[30] K. Hirai, M. Hirose, Y. Haikawa, T. Takenaka, The development of honda humanoid robot, in: Robotics and Automation, 1998. Proceedings. 1998 IEEE International Conference on, Vol. 2, 1998, pp. 1321 –1326 vol.2.
[31] T. McGeer, Passive dynamic walking, International Journal of Robotics Research 9 (2) (1990) 62–82.
[32] J. Pratt, Exploiting inherent robustness and natural dynamics in the control of bipedal walking robots, Ph.D. thesis, Massachusetts Institute of Technology (June 2000).
[33] S. Whittlesey, R. Van Emmerik, J. Hamill, The swing phase of human walking is not a passive movement, Motor Control 4 (2000) 273–292.
[34] T. Ryschon, M. Fowler, R. Wysong, A. Anthony, S. Balaban, Efficiency of human skeletal muscle in vivo: comparison of isometric, concentric, and eccentric muscle action, Journal of Applied Physiology 83 (1997) 867–874.
[35] M. Spong, M. Vidyasagar, Robot Dynamics and Control, John Wiley and Sons, 1989.